Solution of the general dynamic equation along approximate fluid trajectories generated by the method of moments

Rob Hagmeijer,[a] Rutger H. A. IJzermans, and Frits Put
Department of Mechanical Engineering, University of Twente, P.O. Box 217, 7500 AE Enschede, The Netherlands

(Received 30 April 2004; accepted 1 April 2005; published online 6 May 2005)

We consider condensing flow with droplets that nucleate and grow, but do not slip with respect to the surrounding gas phase. To compute the local droplet size distribution, one could solve the general dynamic equation and the fluid dynamics equations simultaneously. To reduce the overall computational effort of this procedure by roughly an order of magnitude, we propose an alternative procedure, in which the general dynamic equation is initially replaced by moment equations complemented with a closure assumption. The key notion is that the flow field obtained from this so-called method of moments, i.e., solving the moment equations and the fluid dynamics equations simultaneously, approximately accommodates the thermodynamic effects of condensation. Instead of estimating the droplet size distribution from the obtained moments by making assumptions about its shape, we subsequently solve the exact general dynamic equation along a number of selected fluid trajectories, keeping the flow field fixed. This alternative procedure leads to fairly accurate size distribution estimates at low cost, and it eliminates the need for assumptions on the distribution shape. Furthermore, it leads to the exact size distribution whenever the closure of the moment equations is exact. © *2005 American Institute of Physics*. [DOI: 10.1063/1.1921147]

I. INTRODUCTION

Condensing flows play different roles in industrial machinery such as steam turbines and supersonic gas conditioners. In the low pressure stages of steam turbines condensation is unfavorable since it decreases the turbine efficiency. In contrast, condensation is essential in supersonic gas conditioners since it provides, together with vortex generation, the mechanism to separate chemical components of a compound gas. In both examples it is required to predict the droplet size distributions accurately.

During the last two decades, various authors have calculated droplet size distributions in air-water flows based on simultaneous solution of the fluid dynamics equations (FDEs) and the general dynamic equation (GDE), a conservation equation for the droplet number density in phase space.[1–5] All of these authors employ an Eulerian description of the FDEs combined with a Lagrangian description of the GDE. Two of the main advantages of this mixed Eulerian–Lagrangian approach are[4] (i) the discretization of the Lagrangian description of droplet dynamics is expected to be quite accurate since it follows single droplets step by step, and (ii) in contrast to an overall Eulerian approach, it circumvents the necessity of an extremely fine mesh in and around the nucleation zone. Two disadvantages, however, can also be mentioned: (i) a large number of fluid trajectories have to be tracked frequently, and (ii) data have to be interpolated frequently between the Lagrangian and Eulerian coordinate systems.

As an efficient approximation, several authors have employed the so-called method of moments (MOM) to calculate condensing air-water flows.[6–9] The MOM consists of simultaneous solution of the FDEs and a number of moment equations (MEs) that are obtained from taking moments of the GDE. The main advantage of the ME/FDE approach with respect to the GDE/FDE approach is the strong reduction of computational effort. Two apparent disadvantages, however, are (i) the necessity of a closure model, and/or (ii) the required assumptions on the shape of the distribution function. It is noted that these two disadvantages coincide when closure is obtained by assuming a generic size distribution. Several closure techniques have been used in the literature. White and Hounslow[9] use a growth law that is linear in the droplet radius that allows for exact closure. This is confirmed by their comparison of calculated moments from both the ME/FDE approach and the GDE/FDE approach, showing almost identical results. Hill[6] employs the Hertz–Knudsen growth law and obtains closure of the MEs by observing that the growth rate is almost independent of the droplet radius for larger radii, leading to a mean growth rate approximation. The same method is used by Adam and Schnerr.[7] McCallum and Hunt[8] apply a similar approach to an alternative growth law.

Within the field of aerosol dynamics a large range of closure methods has been developed. All of the ME/FDE approaches resulting from aerosol investigations are designed to cope with coagulation and segregation, in addition to nucleation and growth. One way of closure is to assume a generic shape of the droplet size distribution, e.g., "log-normal," "(modified) γ," Laguerre polynomials expansion, or associate Laguerre polynomials expansion.[10–15] Alternatively, Barrett and Jheeta[16] assume a functional form of the moments instead of the size distribution itself, and

[a]Author to whom correspondence should be addressed. Electronic mail: r.hagmeijer@ctw.utwente.nl

McGraw[17] uses a quadrature expression for the moments. Finally, Frenklach[18] introduces a more complex interpolative closure.

To assess the accuracy of the moments obtained by the MOM with various closure models, Barrett and Webb[19] present a comparison with data obtained from the GDE/FDE approach, revealing errors of typically a few percent for the cases considered. This suggests that the MOM is fairly suitable to estimate averages of the size distribution *and* to estimate the thermodynamic effects of condensation on the flow field.

Estimating the size distribution itself from these data by means of generic shape assumptions is, however, not straightforward. It has been found that the widely used log-normal and (modified) γ distributions belong to classes of multiple distributions having identical moments.[20,21] Although McGraw *et al.*[21] found that the physical and optical properties and dynamics of these multiple distributions are virtually identical, there is a need to improve the accuracy of distribution predictions when details of such distributions are important.

Close inspection of the GDE/FDE approach on the one hand, and the ME/FDE approach on the other hand, learns that three major differences between these two approaches can be identified.

(i) The GDE/FDE approach leads to a detailed description of the droplet size distribution, whereas the ME/FDE approach leads to approximate moments of this distribution.

(ii) The GDE/FDE approach leads to accurate descriptions of the velocity, pressure, and temperature fields, whereas the ME/FDE approach leads to approximations of these fields.

(iii) The computational effort related to the GDE/FDE approach is approximately one order of magnitude larger than the computational effort related to the ME/FDE approach.

In the present work we investigate the possibility to solve the GDE approximately, whereas the computational effort is strongly reduced. We consider condensing flow including nucleation and growth, with droplets that are assumed not to slip with respect to the surrounding gas phase. The key notion we make is that the velocity, pressure, and temperature fields obtained from the ME/FDE approach approximately accommodate the thermodynamic effects of condensation. Moreover, whenever the closure of the MEs is exact, the accommodation of thermodynamic effects is also exact. We use the velocity field obtained from the ME/FDE approach to generate approximate fluid trajectories and solve the GDE along these trajectories, leading to a detailed droplet size distribution. The related computational effort of this procedure is proportional to that of the ME/FDE approach, which will typically take 90% of the total computational effort. Three disadvantages related to the conventional approach are eliminated in this way: (i) only a limited number of fluid trajectories has to be considered, (ii) interpolation from the Lagrangian coordinate system to the Eulerian coordinate system is not required, and (iii) additional assumptions on the generic distribution shape are not required to estimate the actual size distribution. Furthermore, in the limit of exact closure of the MEs, the proposed procedure leads to the exact size distribution.

II. GOVERNING EQUATIONS

A. Fluid dynamic equations

The FDEs are based on conservation of mass, momentum, and energy in physical space. In the present work we assume that viscous stresses and heat conduction are negligible. As a consequence, we use the Euler equations instead of the Navier–Stokes equations:

$$\frac{\partial}{\partial t}(\rho) + \frac{\partial}{\partial x_j}(\rho u_j) = 0, \tag{1}$$

$$\frac{\partial}{\partial t}(\rho u_i) + \frac{\partial}{\partial x_j}(\rho u_i u_j + \delta_{ij} p) = 0, \quad i = 1,2,3, \tag{2}$$

$$\frac{\partial}{\partial t}(\rho E) + \frac{\partial}{\partial x_j}(\rho u_j H) = 0. \tag{3}$$

The symbols x_j and u_j represent the jth components of the position and velocity vectors in physical space, respectively. Furthermore, ρ is the mass density, p is the pressure, ρE is the total energy density (internal energy and kinetic energy), and ρH is the total enthalpy density.

B. General dynamic equation

The composition of a condensing gas-vapor mixture at a certain location $\boldsymbol{x}$ and time instant t in terms of the number of droplets per unit volume, and the distribution of these droplets over a range of radii, is conveniently described by the radius distribution function $f(r,\boldsymbol{x},t)$. The distribution function is defined such that for any given $r>0$, $\boldsymbol{x}\in\mathbb{R}$, and $t>0$, the number of droplets per unit volume at time t, at position $\boldsymbol{x}$, with radii smaller than r, is given by

$$N(r,\boldsymbol{x},t) = \int_0^r f(r',\boldsymbol{x},t)dr'. \tag{4}$$

The distribution function f is governed by the GDE, which is based on droplet number conservation in phase space. For the derivation of the GDE we refer to standard textbooks on the subject, e.g., Refs. 22 and 23. In absence of slip, coagulation, and segregation, the GDE is

$$\frac{\partial f}{\partial t} + \frac{\partial}{\partial r}(\dot{r} f) + \frac{\partial}{\partial x_j}(u_j f) = \delta(r - r^*)J. \tag{5}$$

Here $\dot{r}(r,\boldsymbol{x},t)$ is the growth rate of droplets, $r^*(\boldsymbol{x},t)$ is the critical radius, i.e., the radius at which droplets nucleate, and $J(\boldsymbol{x},t)$ is the nucleation rate per unit volume. Finally, δ represents the Dirac delta function.

The liquid mass fraction, denoted by g, is defined as the ratio of mass contained in droplets on the one hand, and mass contained in the fluid on the other hand:

$$g \equiv \rho_\ell/\rho. \tag{6}$$

Here ρ_ℓ is the liquid mass density taken over a small mixture volume containing sufficiently many droplets, and ρ is the mixture mass density. Upon assuming spherical droplets, the liquid mass fraction is related to the third moment of the droplet radius distribution function:

$$g \equiv \frac{\rho_L}{\rho}\frac{4}{3}\pi\int_0^\infty r^3 f dr, \tag{7}$$

where ρ_L is the liquid mass density within a single droplet.

The GDE and the FDEs are coupled by the pressure p, the nucleation rate J, and the growth rate $\dot{r}$:

$$p = p(\rho, \rho u, \rho v, \rho w, \rho E, g), \tag{8}$$

$$J = J(\rho, \rho u, \rho v, \rho w, \rho E, g), \tag{9}$$

$$\dot{r} = \dot{r}(\rho, \rho u, \rho v, \rho w, \rho E, g, r). \tag{10}$$

Simultaneous solution of the GDE and the FDEs leads to accurate size distributions, and velocity, pressure, and temperature fields. The model is completed by the relations for thermodynamics, droplet nucleation, and droplet growth, which are given in Appendixes A and B, respectively.

C. Moment equations

To obtain the MEs, we multiply the GDE by r^k, with k an integer, and integrate from $r=0$ to $r=\infty$:

$$\frac{\partial \mu_k}{\partial t} + \int_0^\infty r^k \frac{\partial}{\partial r}(\dot{r} f) dr + \frac{\partial}{\partial x_j}(u_j \mu_k) = (r^*)^k J. \tag{11}$$

The kth moment μ_k is defined as

$$\mu_k \equiv \int_0^\infty r^k f dr. \tag{12}$$

Several authors express the moments in terms of integrals over time instead of integrals over the radius. It has been demonstrated in Ref. 24, however, that both formulations are equivalent and, moreover, consistent with the GDE. The remaining integral can be further evaluated:

$$\int_0^\infty r^k \frac{\partial}{\partial r}(\dot{r} f) dr = [r^k \dot{r} f]_0^\infty - k\int_0^\infty r^{k-1}\dot{r} f dr. \tag{13}$$

The first term on the right-hand side is zero since droplets with zero radius or infinite radius do not exist. The second term on the right-hand side is written as

$$k\int_0^\infty r^{k-1}\dot{r} f dr = k\alpha_{k-1}\mu_{k-1}, \tag{14}$$

with

$$\alpha_m \equiv \frac{1}{\mu_m}\int_0^\infty r^m \dot{r} f dr. \tag{15}$$

As a result, the first $M+1$ moment equations become

$$\frac{\partial \mu_k}{\partial t} + \frac{\partial}{\partial x_j}(u_j \mu_k) = (r^*)^k J + k\alpha_{k-1}\mu_{k-1}, \qquad k = 0,1,2,\ldots,M. \tag{16}$$

This set forms a closed system when the α_m are known for $m=0,1,2,\ldots,M-1$. Upon modeling the α_m in terms of the other variables, one can approximately close the system of equations. The closure method applied in the present investigation is due to Hill,[6] which is explained in Appendix B 3. Since the liquid mass fraction is related to the third moment, viz., Eq. (7), we take $M=3$.

The method of moments consists of simultaneous solution of the MEs and the FDEs, leading to approximate moments of the droplet size distribution, and approximations of the velocity, pressure, and temperature fields. The conventional method to estimate the size distribution from the moments obtained, consists of assuming a generic distribution shape. In the present paper we use the log-normal assumption to compare the results obtained from the method of moments, with the results obtained from the alternative method proposed in Sec. III. The log-normal distribution is described in Appendix C.

III. SOLUTION OF GDE ALONG TRAJECTORIES

In this section, we describe how to solve the GDE along approximate fluid trajectories generated by the ME/FDE approach, in order to obtain size distribution estimates without making any assumptions about the distribution shape.

A. Preintegration of the GDE

To solve the GDE along fluid trajectories, we first preintegrate the GDE over the radius, along phase paths. We define a phase path in terms of a set of four functions of time: the three spatial coordinates $\overline{\boldsymbol{x}}(t;\boldsymbol{x}_1,t_1)$, and the radius coordinate $\overline{r}(t;r_1,\boldsymbol{x}_1,t_1)$, defined as the solutions of two coupled boundary value problems:

$$\frac{d\overline{\boldsymbol{x}}}{dt} = \boldsymbol{u}(\overline{\boldsymbol{x}},t), \quad \overline{\boldsymbol{x}}(t_1;\boldsymbol{x}_1,t_1) = \boldsymbol{x}_1, \tag{17}$$

and

$$\frac{d\overline{r}}{dt} = \dot{r}(\overline{r},\overline{\boldsymbol{x}},t), \quad \overline{r}(t_1;r_1,\boldsymbol{x}_1,t_1) = r_1. \tag{18}$$

Hence, $\overline{\boldsymbol{x}}$ describes the time evolution of the position of a droplet with position $\boldsymbol{x}_1$ at $t=t_1$, and $\overline{r}$ describes the time evolution of the radius of that droplet with radius r_1 at $t=t_1$. It is noted that the phase path is also well defined for $t<t_1$.

These definitions enable one to write the GDE in a Lagrangian form. We first employ the mass conservation equation, Eq. (1), to rewrite the GDE as

$$\frac{\partial \hat{f}}{\partial t} + \frac{\partial}{\partial r}(\dot{r}\hat{f}) + u_j\frac{\partial \hat{f}}{\partial x_j} = \delta(r-r^*)\hat{J}, \tag{19}$$

where $\hat{f} \equiv f/\rho$ and $\hat{J} \equiv J/\rho$. We then integrate Eq. (19) over r,

$$\frac{\partial \hat{N}}{\partial t} + [\dot{r}\hat{f}]_0^r + u_j\frac{\partial \hat{N}}{\partial x_j} = H(r-r^*)\hat{J}, \tag{20}$$

where $\hat{N} \equiv N/\rho$ and H represents the Heaviside step function. Since

$$f(0,\boldsymbol{x},t)=0, \quad \forall\, \boldsymbol{x},t, \tag{21}$$

and recognizing from Eq. (4) that $\hat{f}\equiv\partial\hat{N}/\partial r$, we obtain from Eq. (20) a differential equation for $\hat{N}(r,\boldsymbol{x},t)$:

$$\frac{\partial\hat{N}}{\partial t}+\dot{r}\frac{\partial\hat{N}}{\partial r}+u_j\frac{\partial\hat{N}}{\partial x_j}=H(r-r^*)\hat{J}. \tag{22}$$

This equation expresses the balance between the time change of the number of droplets per unit mass with radii smaller than r on the one hand, and growth, convection, and nucleation on the other hand. Along the phase path $(r,x,t)=(\overline{r},\overline{\boldsymbol{x}},t)$ we have

$$\frac{\partial\hat{N}}{\partial t}+\dot{r}\frac{\partial\hat{N}}{\partial r}+u_j\frac{\partial\hat{N}}{\partial x_j}\equiv\frac{d}{dt}\hat{N}(\overline{r},\overline{\boldsymbol{x}},t), \tag{23}$$

leading to

$$\frac{d}{dt}\hat{N}(\overline{r},\overline{\boldsymbol{x}},t)=H[\overline{r}-r^*(\overline{\boldsymbol{x}},t)]\hat{J}(\overline{\boldsymbol{x}},t). \tag{24}$$

The Heaviside step function enforces that, along phase paths, the time increase of the number of droplets per unit mass with radii smaller than $\overline{r}$ is equal to the nucleation rate per unit mass when $\overline{r}>r^*$, but zero when $\overline{r}<r^*$.

Backward time integration of Eqs. (17) and (18) for a single value of $\boldsymbol{x}_1$ and a range of values of r_1 over a time domain $[t_0,t_1]$, and subsequent forward time integration of Eq. (24) along these phase paths, results in the function $\hat{N}(r,\overline{\boldsymbol{x}},t)$ when t_0 is chosen such that $\hat{N}[r,\overline{\boldsymbol{x}}(t_0),t_0]$ is known for all r. For example, one typically chooses t_0 such that $[\overline{\boldsymbol{x}}(t_0),t_0]$ represents a point in the flow domain where there are no droplets at all, i.e., $\hat{N}[r,\overline{\boldsymbol{x}}(t_0),t_0]\equiv 0$. Finally, the distribution function is reconstructed along the fluid path as

$$f[r,\overline{\boldsymbol{x}}(t),t]=\rho[\overline{\boldsymbol{x}}(t),t]\frac{\partial}{\partial r}\hat{N}[r,\overline{\boldsymbol{x}}(t),t], \quad t\in[t_0,t_1]. \tag{25}$$

B. Quasi-1D approximation and discretization

To demonstrate the proposed method, we consider a duct of length L and cross sectional area A, which varies slowly with the axial coordinate x, i.e.,

$$\frac{L}{A}\frac{dA}{dx}\ll 1. \tag{26}$$

The FDEs, Eqs. (1)–(3), and the MEs, Eq. (16), are replaced by quasi-one-dimensional approximations:[25]

$$\frac{\partial}{\partial t}(\rho)+\frac{\partial}{\partial x}(\rho u)=-\rho u\frac{1}{A}\frac{dA}{dx}, \tag{27}$$

$$\frac{\partial}{\partial t}(\rho u)+\frac{\partial}{\partial x}(\rho u^2+p)=-\rho u^2\frac{1}{A}\frac{dA}{dx}, \tag{28}$$

$$\frac{\partial}{\partial t}(\rho E)+\frac{\partial}{\partial x}(\rho uH)=-\rho uH\frac{1}{A}\frac{dA}{dx}, \tag{29}$$

$$\frac{\partial\mu_k}{\partial t}+\frac{\partial}{\partial x}(\mu_k u)=-\mu_k u\frac{1}{A}\frac{dA}{dx}+(r^*)^kJ+k\alpha_{k-1}\mu_{k-1},$$
$$k=0,1,2,\ldots,M. \tag{30}$$

To discretize this quasi-one-dimensional approximation, a standard finite volume method is employed including the Van Leer flux splitting,[26] and the Van Albada flux limiter.[27] The resulting algorithm is second-order accurate in space. The steady state solution is obtained by a fourth order Runge–Kutta time integration scheme, and the nucleation term is resolved by means of fractional time integration. Details of this discretization are given in Ref. 28.

To discretize the one-dimensional formulation of the phase path equations, Eqs. (17) and (18), we choose a point of interest, (r_1,x_1,t_1), and solve the following set of algebraic equations:

$$\overline{x}^{n-1}=\overline{x}^n-u(\overline{x}^n,t^n)\Delta t, \quad \overline{x}^0=x_1, \tag{31}$$

$$\overline{r}^{n-1}=\overline{r}^n-\dot{r}(\overline{r}^n,\overline{x}^n,t^n)\Delta t, \quad \overline{r}^0=r_1, \tag{32}$$

where t^n is defined as

$$t^n=t_1+n\Delta t, \quad n=0,-1,-2,\ldots,-n_0. \tag{33}$$

The value of n_0 is such that $\overline{x}^{-n_0}$ corresponds to the required starting point of the phase path. The preintegrated general dynamic equation, Eq. (24), is discretized as

$$\hat{N}^{n+1}=\hat{N}^n+H[\overline{r}^n-r^*(\overline{x}^n,t^n)]\hat{J}(\overline{x}^n,t^n)\Delta t, \quad \hat{N}^{-n_0}=0. \tag{34}$$

For a given flow solution, Eqs. (31)–(34) are solved subsequently for a number of decreasing values of Δt. Each next value of Δt is half of the previous value of Δt. When the differences between two subsequent solutions are below machine accuracy level [typically $O(10^{-14})$], the last obtained solution is considered sufficiently accurate.

C. Global procedure

In all calculations, we first use the ME/FDE approach that constitutes the MOM. It consists of solving the quasi-one-dimensional form of the FDEs, Eqs. (27)–(29), simultaneously with the quasi-one-dimensional form of the MEs, Eq. (30). As a result, we obtain approximate pressure, temperature, density, velocity, and liquid mass fraction fields. In all cases we close the MEs by employing Hill's approximate growth law. We employ two models for nucleation: (i) the conventional model without denucleation and (ii) an alternative model obtained by replacing J by $H(-Dr^*/Dt)J$, see Appendix B 4. We denote these methods by MOM^0 and MOM^+, respectively.

Second, we continue by means of a phase path analysis (PPA) by solving the Lagrangian form of the GDE, Eq. (24), along a range of phase paths to reconstruct the droplet radius distribution along a fluid trajectory. We use two different growth laws within PPA: (i) Hill's approximate growth law and (ii) the Hertz–Knudsen (HK) growth law, see Appendix B 2. We denote these methods by PPA-Hill and PPA-HK, respectively.

The moments directly resulting from MOM^0 or MOM^+ on the one hand, and the moments indirectly resulting from

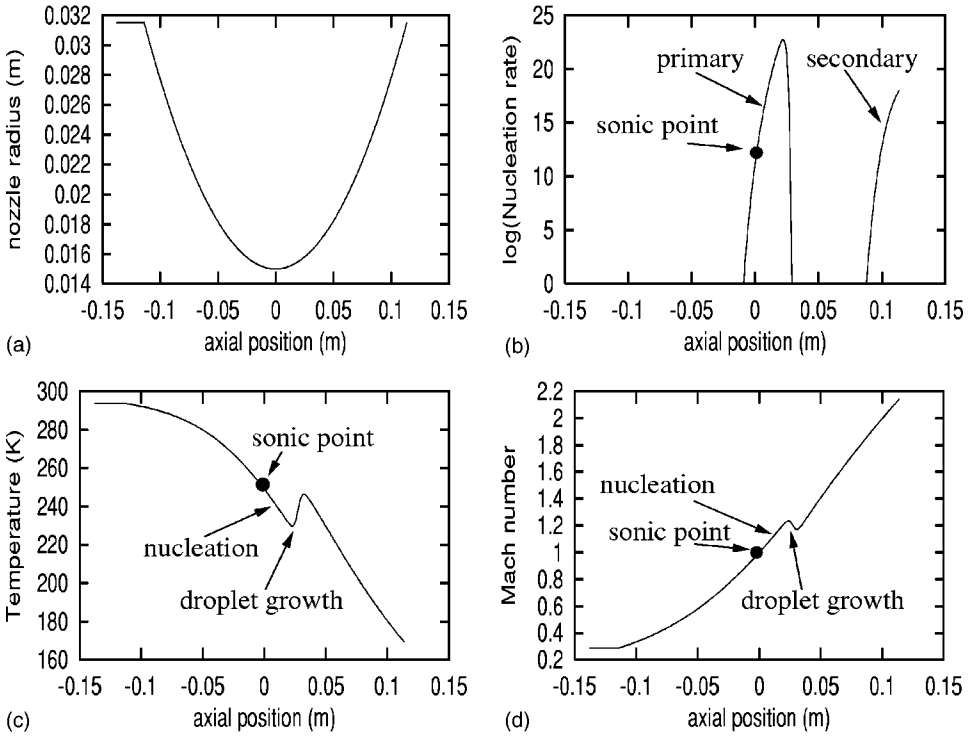

FIG. 1. Typical characteristics of condensing flow in a symmetric nozzle: (a) Nozzle radius, (b) nucleation rate, (c) temperature, and (d) Mach number.

PPA-Hill or PPA-HK by integration of the obtained distribution function on the other hand, are compared to assess the relative accuracy of the two methods. It is noted that exact closure of the method of moments implies exact calculation of the distribution function. As a result, MOM^0 and MOM^0/PPA-Hill should give identical results for the moments.

Finally, we also estimate the size distribution from the obtained moments from MOM^0 by assuming a log-normal shape, labeled as MOM^0/log-normal, and compare it to the size distribution obtained from PPA.

IV. TEST CASE DESCRIPTION AND RESULTS

To test the proposed method we consider the condensing flow of air-water mixtures through a symmetric nozzle. Two different values for the water content g_{max} are considered: (1) "Lower water content case," $g_{max}=8.18$ g/kg; (2) "higher water content case," $g_{max}=20.50$ g/kg.

The contour of the nozzle is depicted in Fig. 1(a), while typical graphs of the nucleation rate J, the temperature T, and the Mach number M as functions of the axial coordinate x are depicted in Figs. 1(a)–1(d). Two nucleation zones are observed: primary nucleation starting just in front of the throat of the nozzle and secondary nucleation at the end of the diverging part of the nozzle. It is noted that the scale of J is logarithmic and that the primary nucleation peak is about five orders of magnitude larger than the secondary one. Droplet nucleation and droplet growth cause the temperature and the Mach number to locally increase and decrease, respectively. This is in contrast with the situation of a noncondensing expanding gas in a supersonic diverging channel. The reason for this contrasting behavior is the heat release of the growing droplets.

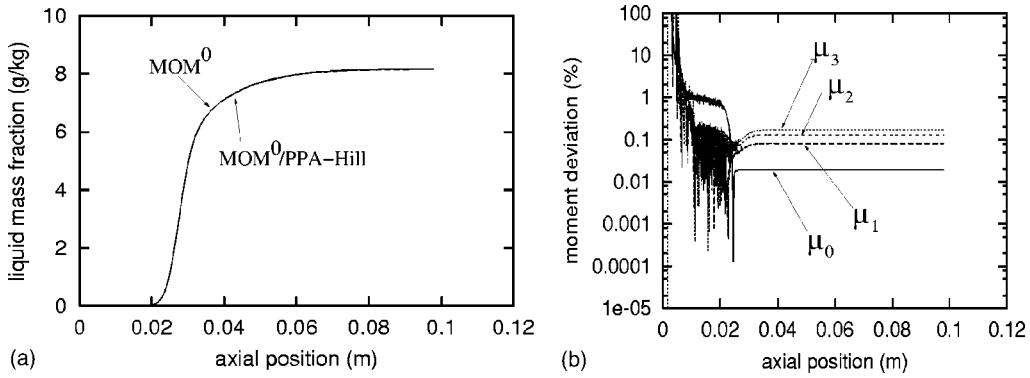

FIG. 2. Liquid mass fraction and relative moment deviations between MOM^0 and MOM^0/PPA-Hill for $g_{max}=8.18$ g/kg: (a) Liquid mass fraction and (b) relative deviation in all moments.

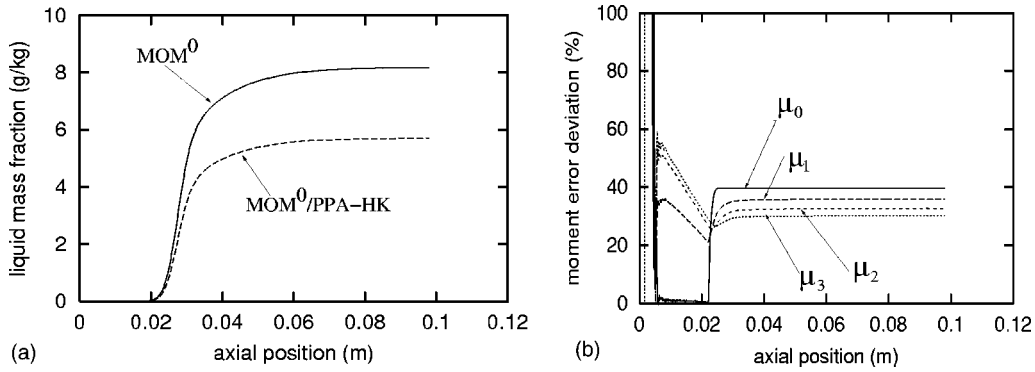

FIG. 3. Liquid mass fraction and relative moment deviations between MOM^0 and MOM^0/PPA-HK for $g_{max}=8.18$ g/kg: (a) Liquid mass fraction and (b) relative deviation in all moments.

A. Lower water content case

We start with the lower water content case $g_{max}=8.18$ g/kg. To verify our algorithms, we compare liquid mass fraction data obtained directly from the method of moments to similar data obtained from the phase path analysis, using Hill's approximation of the droplet growth law. Under these conditions both methods should theoretically give identical data, since the simplified growth law enables exact closure of the moment equations. Figure 2(a) shows the liquid mass fractions obtained from MOM^0 and PPA-Hill, respectively, and Fig. 2(b) shows the relative deviation in all of the four moments. In the region where $g>1$ g/kg all errors are $\approx 0.1\%$ or less. This is considered a sufficiently accurate verification since accurate integration of the nucleation rate is a challenge in itself due to the extremely large gradients.

To assess the validity of the proposed method we now apply the phase path analysis with the Hertz–Knudsen growth law, which is more complete than Hill's approximate growth law. Figure 3(a) shows the liquid mass fractions obtained from MOM^0 and from PPA-HK, respectively. Figure 3(b) shows the relative deviation in all of the four moments.

In the region where $g>1$ g/kg, the deviations are 30%–40%. One of the main reasons for the relatively large discrepancy between the moments obtained from MOM^0 on the one hand and from PPA-HK on the other hand, is that, within MOM^0, denucleation is not accounted for. In contrast, within PPA-HK, droplets that have radii smaller than the critical radius r^* will shrink and eventually will evaporate completely. Therefore we replace MOM^0 by MOM^+ to approximately account for denucleation, and compare the moments again. Figure 4(a) shows the liquid mass fractions obtained from MOM^+ and from PPA-HK, respectively. Figure 4(b) shows the relative deviation in all of the four moments. In the region where $g>1$ g/kg, the deviations are 10%–20%, indicating a significant improvement compared to the MOM^0/PPA-HK combination.

An impression of the distribution function at various axial positions related to the three methods considered is presented in Figs. 5(a)–5(f) and 6(a)–6(f), respectively. We have scaled the droplet radius by μ_1/μ_0 and the distribution function by μ_0^2/μ_1, respectively, implying that the mean scaled radius is identical to 1, and that the integral of the scaled distribution function is also identical to 1. Figures 5(a)–5(f) show a comparison of the distribution function obtained from MOM^0/PPA-Hill on the one hand and the distribution function obtained from MOM^0 assuming a log-normal representation on the other hand. The log-normal assumption is reasonable for the downstream positions ($x \geqslant 2.8$ cm) but fails at the positions where nucleation is still active ($x=2.0$ cm, $x=2.5$ cm).

A similar comparison of the size distribution function obtained with MOM^0/PPA-Hill and the two results obtained with MOM^0/PPA-HK and MOM^+/PPA-HK, respectively, is presented in Figs. 6(a)–6(f). The apparent skewness and

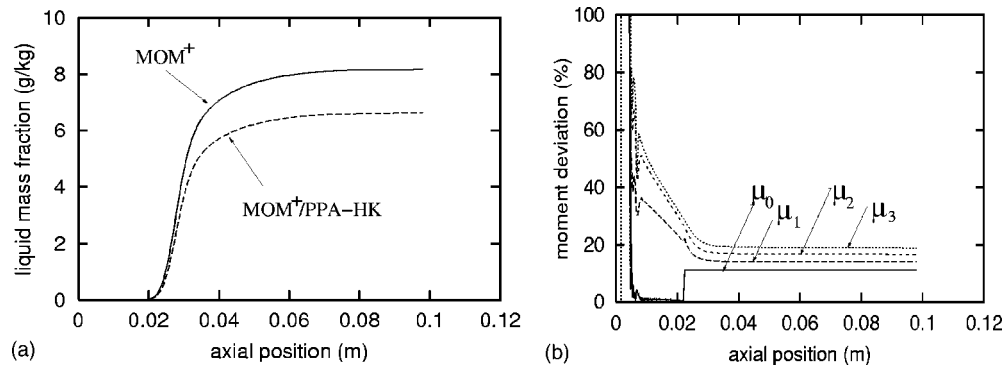

FIG. 4. Liquid mass fraction and relative moment deviations between MOM^+ and MOM^+/PPA-HK for $g_{max}=8.18$ g/kg: (a) Liquid mass fraction and (b) relative deviation in all moments.

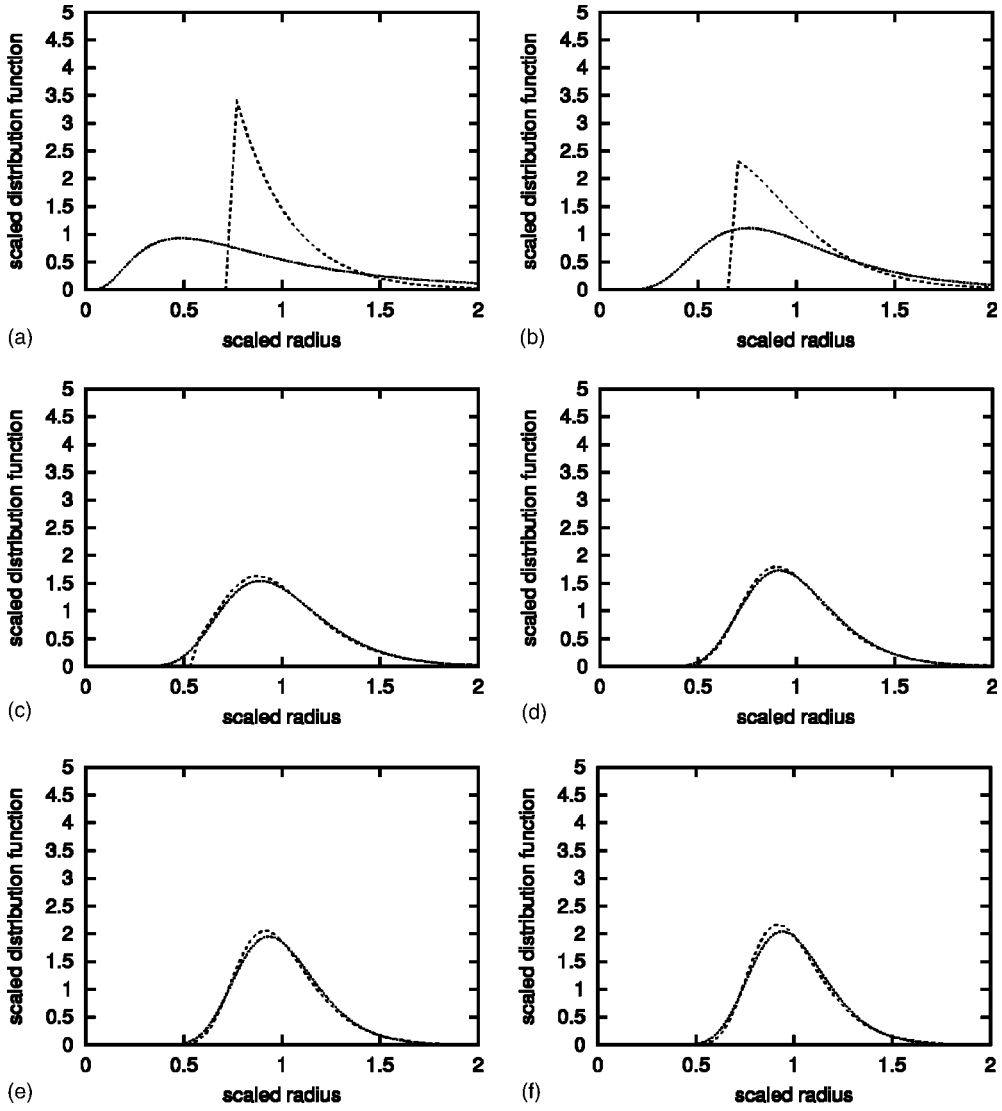

FIG. 5. Scaled distribution function from MOM^0/PPA-Hill (short dashes) and MOM^0/log-normal (dotted) at various axial positions for $g_{max}=8.18$ g/kg: (a) $x=2.0$ cm, (b) $x=2.5$ cm, (c) $x=2.8$ cm, (d) $x=3.0$ cm, (e) $x=4.0$ cm, and (f) $x=11.37$ cm.

slenderness of the distribution function obtained with the Hertz–Knudsen growth law (PPA-HK) is in contrast with the more symmetric distribution obtained with Hill's approximation of the Hertz–Knudsen growth law (PPA-Hill).

B. Higher water content case

For the higher water content case $g_{max}=20.50$ g/kg we present a completely similar analysis. The corresponding curves are presented in Figs. 7–11. From these figures it appears that similar observations can be made. The improvement in accuracy, however, indicated by Fig. 9, due to our crude model for denucleation is even stronger than for the lower water content case: the deviations in the moments reduce from 30%–40% to ≈10%. Figure 10 shows that the log-normal distribution function assumption is reasonable for all axial positions except for the first one ($x=2.0$ cm). Finally, Fig. 11 confirms the relative skewness and slenderness of the distribution function obtained with the Hertz–Knudsen growth law (PPA-HK), compared to the more symmetric distribution obtained with Hill's approximation of the Hertz–Knudsen growth law (PPA-Hill).

V. CONCLUSIONS

The proposed method of combining the method of moments, i.e., simultaneous solution of the moment equations and the fluid dynamics equations, with phase path analysis, i.e., solution of the general dynamic equation along a fluid trajectory, has demonstrated its potential to approximately reconstruct the droplet size distribution. Whenever the closure of the moments equations is exact, the reconstructed distribution function is also exact. This has been verified by employing Hill's approximate growth law in both the method of moments as well as in the phase path analysis.

Although closure of the method of moments by means of Hill's approximate growth law and subsequent phase path analysis with the Hertz–Knudsen growth law leads to fairly

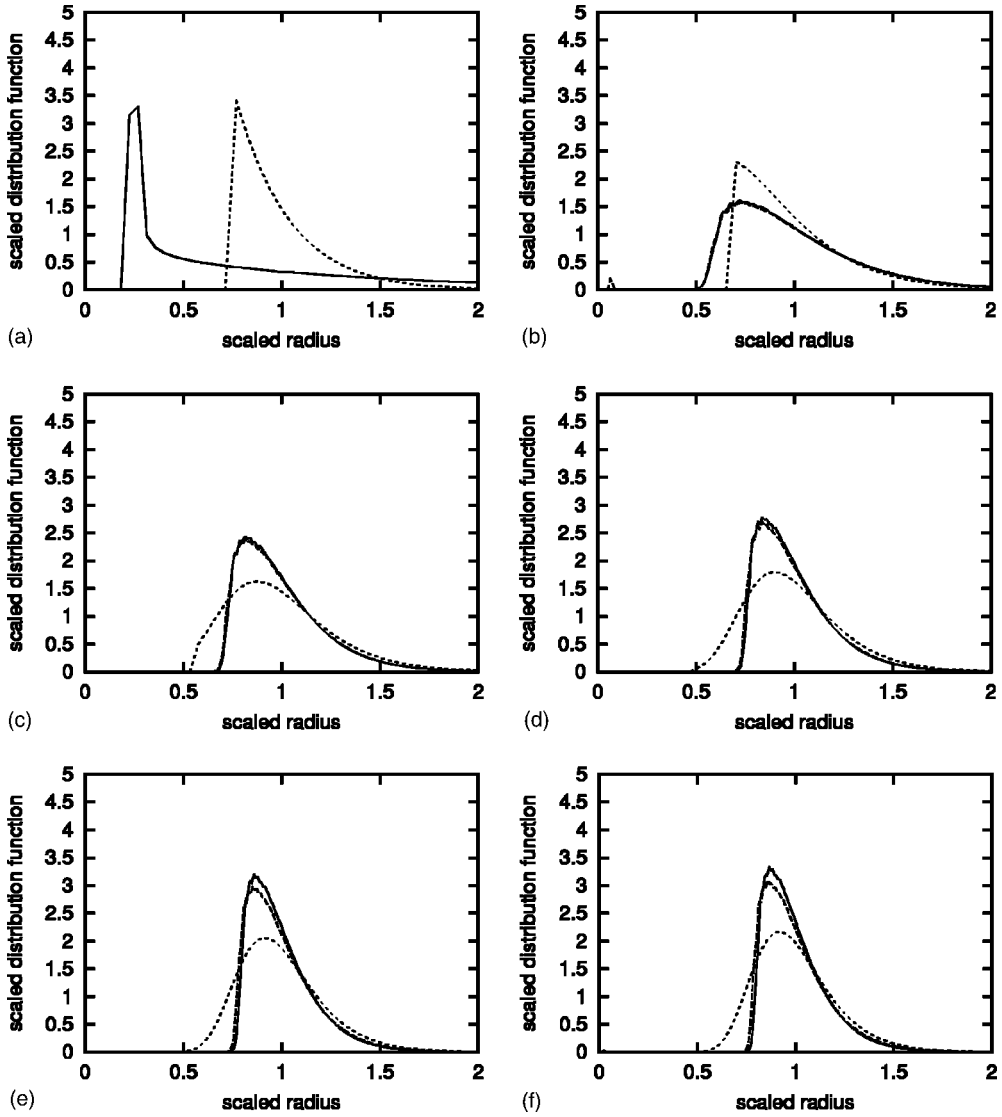

FIG. 6. Scaled distribution function from MOM^0/PPA-Hill (short dashes), MOM^0/PPA-HK (long dashes), and MOM^+/PPA-HK (solid) at various axial positions for $g_{max}=8.18$ g/kg: (a) $x=2.0$ cm, (b) $x=2.5$ cm, (c) $x=2.8$ cm, (d) $x=3.0$ cm, (e) $x=4.0$ cm, and (f) $x=11.37$ cm.

large deviations of 30%–40% in the moments, it has been shown that addition of a rather crude representation of denucleation already results in a significant reduction of these deviations to ≈20% or even 10%.

APPENDIX A: THERMODYNAMICS

We assume that both the inert carrier gas, denoted by the subscript a, and the vapor, denoted by subscript v, are ther-

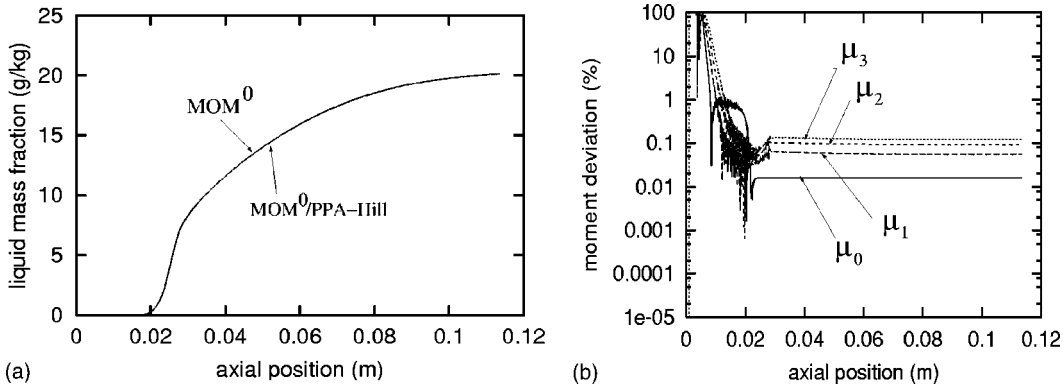

FIG. 7. Liquid mass fraction and relative moment deviations between MOM^0 and MOM^0/PPA-Hill for $g_{max}=20.50$ g/kg: (a) Liquid mass fraction and (b) relative deviation in all moments.

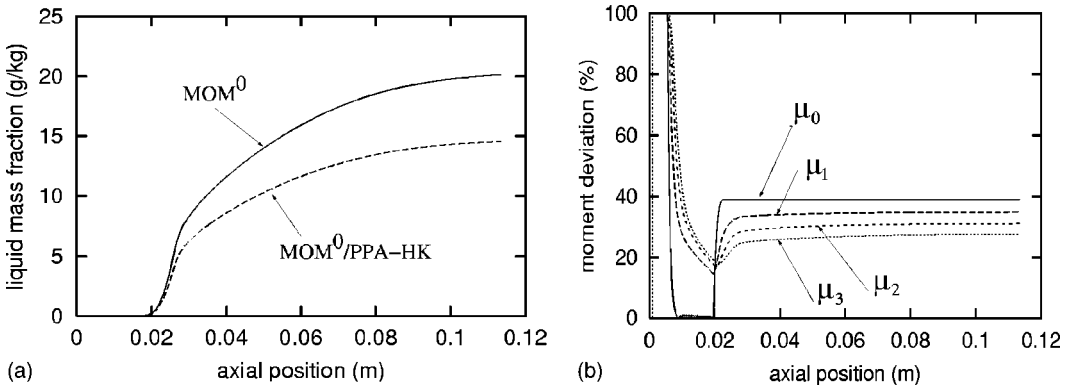

FIG. 8. Liquid mass fraction and relative moment deviations between MOM^0 and MOM^0/PPA-HK for $g_{\max}=20.50$ g/kg: (a) Liquid mass fraction and (b) relative deviation in all moments.

mally perfect gases. Furthermore, we assume that the gas and the vapor are in thermal equilibrium with the liquid droplets. The pressure satisfies

$$p=\rho RT, \quad R=\frac{\rho_a}{\rho}R_a+\frac{\rho_v}{\rho}R_v, \tag{A1}$$

where ρ_a and ρ_v are the mass densities, and R_a and R_v are the gas constants of the two components, respectively. Due to the no-slip assumption, the sum of the liquid mass density ρ_ℓ and the vapor mass density ρ_v satisfies

$$\frac{\partial}{\partial t}\left(\frac{\rho_v+\rho_\ell}{\rho}\right)+u_j\frac{\partial}{\partial x_j}\left(\frac{\rho_v+\rho_\ell}{\rho}\right)=0. \tag{A2}$$

Defining $g_{\max}\equiv(\rho_v+\rho_\ell)/\rho$, this shows that $g_{\max}$ is constant along fluid trajectories. We assume that at inflow boundaries $g_{\max}$ is uniform, which makes $g_{\max}$ a global constant and an upper bound for g everywhere in the flow field:

$$0\leqslant g\leqslant g_{\max}. \tag{A3}$$

From these observations it follows that the densities of the gas and vapor components are related to the overall mass density ρ by

$$\rho_a=(1-g_{\max})\rho, \quad \rho_v=(g_{\max}-g)\rho, \tag{A4}$$

leading to the following expression for the pressure:

$$p=\rho RT, \quad R=(1-g_{\max})R_a+(g_{\max}-g)R_v. \tag{A5}$$

To obtain an expression for the temperature we employ the specific energy of the mixture,

$$e\equiv E-\tfrac{1}{2}u_ju_j \tag{A6}$$

and express it in terms of contributions from the three components:

$$e=\frac{\rho_a}{\rho}e_a+\frac{\rho_v}{\rho}e_v+\frac{\rho_\ell}{\rho}e_L, \tag{A7}$$

where e_a, e_v, and e_L are the internal specific energies of the gas, the vapor, and the liquid, respectively. We assume that the inert carrier gas and the vapor are calorically perfect:

$$e_a=C_v^aT, \quad e_v=C_v^vT. \tag{A8}$$

The specific heat coefficients C_v^a and C_v^v of the inert carrier gas and the vapor, respectively, are constants. We express $e_L(T)$ in terms of specific enthalpy,

$$e_L(T)\equiv h_L(T)-p_L/\rho_L\approx h_L(T), \tag{A9}$$

where we have assumed that $p_L/\rho_L\ll h_L$. To eliminate $h_L(T)$ we use the enthalpy of vaporization (or latent heat),

$$h_0(T)\equiv h_v(T)-h_L(T) \tag{A10}$$

and we express $h_v(T)$ as

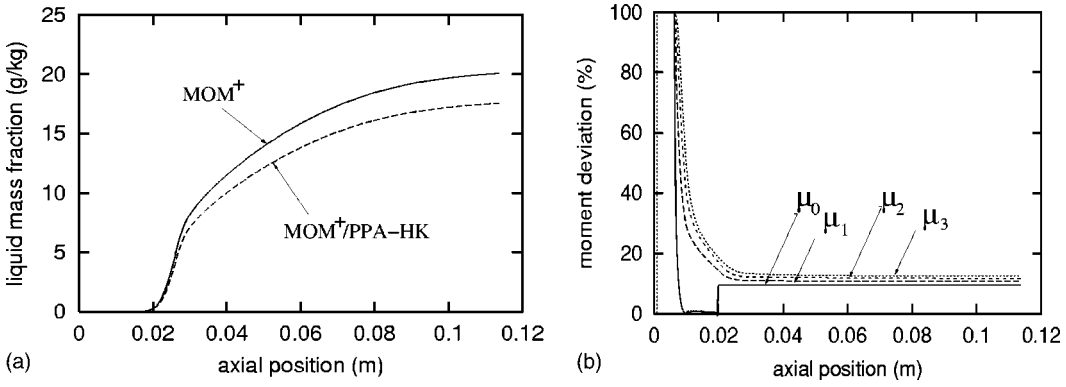

FIG. 9. Liquid mass fraction and relative moment deviations MOM$^+$ and MOM$^+$/PPA-HK for $g_{\max}=20.50$ g/kg: (a) Liquid mass fraction and (b) relative deviation in all moments.

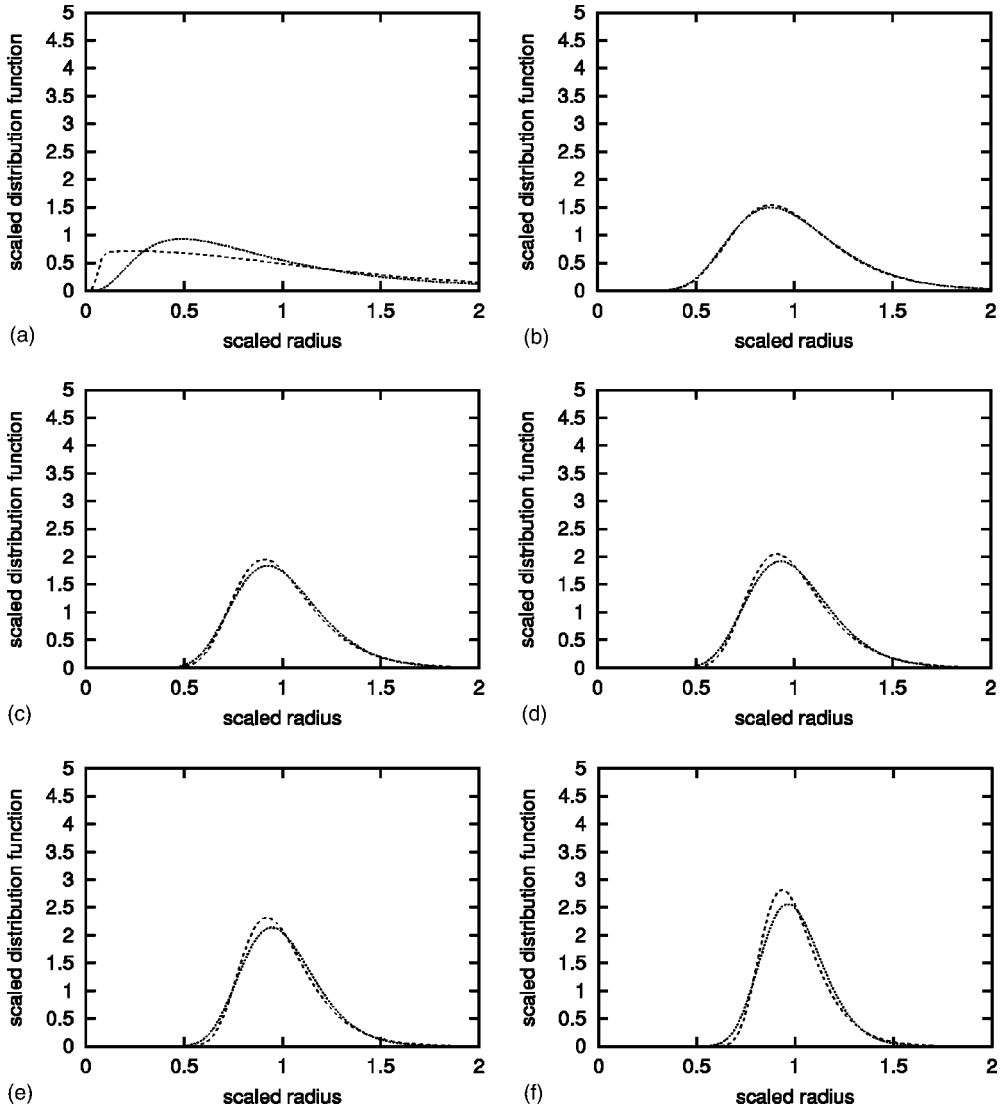

FIG. 10. Scaled distribution function from MOM^0/PPA-Hill (short dashes) and MOM^0/log-normal (dotted) at various axial positions for $g_{\max}=20.50$ g/kg: (a) $x=2.0$ cm, (b) $x=2.5$ cm, (c) $x=2.8$ cm, (d) $x=3.0$ cm, (e) $x=4.0$ cm, and (f) $x=11.37$ cm.

$$h_v(T) \equiv e_v(T) + p_v/\rho_v = e_v(T) + R_v T. \tag{A11}$$

The final result is

$$\begin{aligned} e(T) &= C_v T + gR_v T - gh_0(T), \\ C_v &\equiv (1 - g_{\max})C_v^a + g_{\max}C_v^v, \end{aligned} \tag{A12}$$

which, upon knowledge of the function $h_0(T)$, relates the temperature explicitly to the specific energy.

APPENDIX B: NUCLEATION AND GROWTH

1. Nucleation

Homogeneous nucleation involves the formation of metastable clusters from a population of vapor molecules in a supersaturated state. The rate at which nuclei are formed, per unit volume, J, depends exponentially on the ratio of Gibbs free energy of formation, ΔG^*, and the mean thermal energy kT (viz., e.g., Ref. 29):

$$J = K \exp\left(-\frac{\Delta G^*}{kT}\right), \quad K = \frac{\rho_v^2}{\rho_L}\sqrt{\frac{2\sigma}{\pi m^3}}. \tag{B1}$$

The symbol k is the Boltzmann constant, σ is the surface tension, and m is the mass of a single vapor molecule. Gibbs free energy of formation, ΔG^*, equals

$$\Delta G^* = \tfrac{4}{3}\pi(r^*)^2\sigma. \tag{B2}$$

The symbol r^* represents the critical radius, i.e., the radius of the nuclei that are formed:

$$r^* = \frac{2\sigma}{\rho_L R_v T \ln S}. \tag{B3}$$

Furthermore, S is the saturation ratio, i.e., the ratio of the actual vapor pressure p_v and the saturated vapor pressure $p_s(T)$:

$$S \equiv p_v/p_s(T). \tag{B4}$$

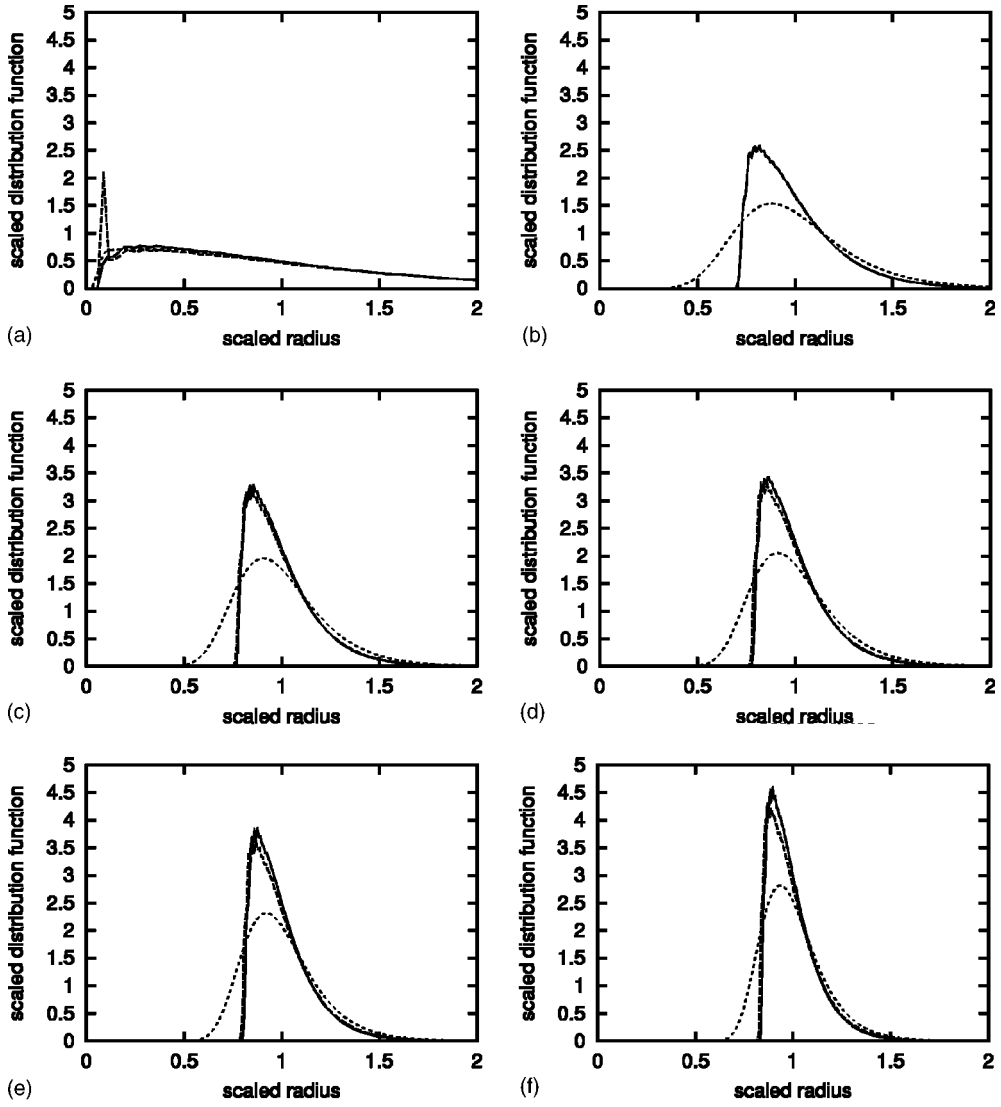

FIG. 11. Scaled distribution function from MOM^0/PPA-Hill (short dashes), MOM^0/PPA-HK (long dashes), and MOM$^+$/PPA-HK (solid) at various axial positions for $g_{\max}=20.50$ g/kg: (a) $x=2.0$ cm, (b) $x=2.5$ cm, (c) $x=2.8$ cm, (d) $x=3.0$ cm, (e) $x=4.0$ cm, and (f) $x=11.37$ cm.

2. Hertz–Knudsen growth law

The Hertz–Knudsen growth law is based on condensation of vapor molecules onto the droplet on the one hand and evaporation of molecules from the droplet on the other hand. The rates of both processes are proportional to the ratio of the relevant vapor pressure and the square root of the mean thermal energy. By taking into account the thermal equilibrium assumption we obtain

$$\dot{r}(r,\boldsymbol{x},t)=\frac{\alpha}{\rho_L}\left(\frac{p_v-p_{s,r}}{\sqrt{2\pi R_v T}}\right). \tag{B5}$$

Here α is the impingement coefficient usually taken equal to 1, and $p_{s,r}$ is the saturated vapor pressure over a curved surface with radius r:

$$p_{s,r}=p_s\exp\left(\frac{2\sigma}{r\rho_L R_v T}\right). \tag{B6}$$

3. Hill's approximation of the Hertz–Knudsen growth law

To close the moment equations for air-water mixtures, Hill[6] introduced an average growth rate for all droplet sizes, based on the observation that, especially for larger radii, the droplet growth rate is in very good approximation independent of the actual droplet radius. The average growth rate is simply obtained by applying the Hertz–Knudsen growth law to a droplet with a characteristic radius r_H defined as

$$r_H(\boldsymbol{x},t)\equiv\sqrt{\frac{\mu_2(\boldsymbol{x},t)}{\mu_0(\boldsymbol{x},t)}}. \tag{B7}$$

As a result we get

$$\dot{r}(r,\boldsymbol{x},t)\approx\dot{r}[r_H(\boldsymbol{x},t),\boldsymbol{x},t]. \tag{B8}$$

This approximation enables one to calculate the coefficients α_m defined by Eq. (15),

$$\alpha_m(\boldsymbol{x},t) = \dot{r}[r_H(\boldsymbol{x},t),\boldsymbol{x},t], \tag{B9}$$

by which the set of moment equations is closed.

4. Denucleation

When the radius of a droplet, r, is smaller than the critical radius r^* the Hertz–Knudsen droplet growth law implies evaporation: the droplet radius decreases with time. In the end, when the droplet radius keeps decreasing, the droplet will disappear completely. We will call this process denucleation. Whenever the critical radius, which is a virtual radius as function of the thermodynamic state, is increasing over a considerable period of time, nuclei will just shrink and disappear. To account for this effect, we propose to replace the nucleation rate J by the following expression:

$$J \to H\left(-\frac{Dr^*}{Dt}\right)J, \tag{B10}$$

where H is the Heaviside step function and D/Dt denotes the material time derivative. As a result, nucleation will be switched off whenever the critical radius r^* is increasing with time in a Lagrangian reference system. This, to some extent, represents denucleation.

To account for massive denucleation when the average growth rate is negative, one could consider to employ the model proposed by Luo[30] that is based on shifting an approximate distribution function over the radius axis in negative direction. In the present work, however, we restrict ourselves to cases with positive average growth rates.

APPENDIX C: LOG-NORMAL SIZE DISTRIBUTION

The log-normal shape is described in, e.g., Ref. 21:

$$f(r,\boldsymbol{x},t) = \frac{\mu_0(\boldsymbol{x},t)}{rs\sqrt{2\pi}}\exp\left\{-\frac{1}{2}\left(\frac{\ln r - m}{s}\right)^2\right\}. \tag{C1}$$

Here, s and m are two parameters that can be expressed in terms of the moments μ_k by using the following relationship:

$$\mu_k = \mu_0 \exp\left\{km + \frac{1}{2}(ks)^2\right\}. \tag{C2}$$

In the present paper we choose μ_0, μ_1, and μ_2 to determine s and m:

$$s^2 = \ln\left(\frac{\mu_0\mu_2}{\mu_1^2}\right), \quad m = \frac{1}{2}\ln\left(\frac{\mu_1^4}{\mu_0^3\mu_2}\right). \tag{C3}$$

[1] F. Bakhtar and M. T. Mohamaddi Tochai, "An investigation of two-dimensional flows of nucleating and wet steam by the time-marching method," Int. J. Heat Fluid Flow **2**, 5 (1980).

[2] M. Moheban and J. B. Young, "A study of thermal non-equilibrium effects in low-pressure wet-steam turbines using a blade-to-blade time-marching technique," Int. J. Heat Fluid Flow **6**, 269 (1985).

[3] S. A. Skillings and R. Jackson, "A robust 'time-marching' solver for one-dimensional nucleating steam flows," Int. J. Heat Fluid Flow **8**, 139 (1987).

[4] J. B. Young, "Two-dimensional, non-equilibrium, wet-steam calculations for nozzles and turbine cascades," J. Turbomach. **114**, 569 (1992).

[5] A. J. White and J. B. Young, "Time marching method for the prediction of two-dimensional unsteady flows of condensing steam," AIAA J. **9**, 579 (1993).

[6] P. G. Hill, "Condensation of water vapor during supersonic expansion in nozzles," J. Fluid Mech. **25**, 593 (1966).

[7] S. Adam and G. Schnerr, "Instabilities and bifurcation of non-equilibrium two-phase flows," J. Fluid Mech. **348**, 1 (1997).

[8] M. McCallum and R. Hunt, "The flow of wet steam in a one-dimensional nozzle," Int. J. Numer. Methods Eng. **44**, 1807 (1999).

[9] A. J. White and M. J. Hounslow, "Modeling droplet size distributions in polydispersed wet-steam flows," Int. J. Heat Mass Transfer **43**, 1873 (2000).

[10] K. W. Lee, "Change of particle size distribution during Brownian coagulation," J. Colloid Interface Sci. **92**, 315 (1983).

[11] M. M. R. Williams, "Some topics in nuclear aerosol dynamics," Prog. Nucl. Energy **17**, 1 (1986).

[12] J. R. Brock and J. Oates, "Moment simulation of aerosol evaporation," J. Aerosol Sci. **18**, 59 (1987).

[13] S. E. Pratsinis, "Simultaneous nucleation, condensation and coagulation in aerosol reactors," J. Colloid Interface Sci. **124**, 416 (1988).

[14] Y. Seo and J. R. Brock, "Distributions for moment simulation of aerosol evaporation," J. Aerosol Sci. **21**, 511 (1990).

[15] M. Kielkiewicz, "Accuracy of the moments method," Ann. Nucl. Energy **21**, 189 (1994).

[16] J. C. Barrett and J. S. Jheeta, "Improving the accuracy of the moments method for solving the aerosol general dynamic equation," J. Aerosol Sci. **27**, 1135 (1996).

[17] R. McGraw, "Description of the aerosol dynamics by the quadrature method of moments," Aerosol Sci. Technol. **27**, 255 (1997).

[18] M. Frenklach, "Method of moments with interpolative closure," Chem. Eng. Sci. **57**, 2229 (2002).

[19] J. C. Barrett and N. A. Webb, "A comparison of some approximate methods for solving the aerosol general dynamic equation," J. Aerosol Sci. **29**, 31 (1998).

[20] W. H. White, "Particle size distributions that cannot be distinguished by their integral moments," J. Colloid Interface Sci. **135**, 297 (1990).

[21] R. McGraw, S. Nemesure, and S. E. Schwartz, "Properties and evolution of aerosols with size distributions having identical moments," J. Aerosol Sci. **29**, 761 (1998).

[22] J. H. Seinfeld, *Atmospheric Chemistry and Physics of Air Pollution* (Wiley, New York, 1986).

[23] M. M. R. Williams and S. K. Loyalka, *Aerosol Science: Theory and Practice* (Pergamon, Oxford, 1991).

[24] R. Hagmeijer, "Equivalence of two different integral representations of droplet distribution moments in condensing flow," Phys. Fluids **16**, 176 (2004).

[25] H. W. Liepmann and A. Roshko, *Elements of Gasdynamics* (Wiley, New York, 1957).

[26] B. van Leer, "Flux-vector splitting for the Euler equations," *Eighth International Conference on Numerical Methods in Fluid Dynamics*, Lecture Notes in Physics (Springer, Berlin, 1982).

[27] G. D. van Albada, B. van Leer, and W. W. Roberts, "A comparative study of computational methods in cosmic gas dynamics," Astron. Astrophys. **108**, 76 (1982).

[28] F. Put, "Numerical simulation of condensation in transonic flows," Ph.D. thesis, University of Twente, 2003.

[29] P. Peeters, J. J. H. Gielis, and M. E. H. van Dongen, "The nucleation behavior of supercooled water vapor in helium," J. Chem. Phys. **117**, 5647 (2002).

[30] X. Luo, "Unsteady flows with phase transition," Ph.D. thesis, Eindhoven University of Technology, 2004.